ROYAL SOCIETY OF CHEMISTRY

Check for updates

Formation mechanisms of hollow manganese hexacyanoferrate particles and construction of a multiple-shell structure†

Fumiyuki Shiba, [ID] *[a] Asumi Yamamoto,[b] Yuuki Shinta,[c] Ushio Mameuda,[a] Yuuki Tahara[c] and Yusuke Okawa [ID] [a]

Formation mechanisms of hollow manganese hexacyanoferrate (Mn-HCF) particles have been investigated. Mn-HCF particles, which were precipitated by mixing an aqueous solution of $K_3[Fe(CN)_6]$ with $MnCl_2$ in the presence of sodium citrate, could be converted into a hollow structure just by washing with distilled water. The powder X-ray diffractometry suggested that the as-prepared particle has a core/shell morphology with different crystal structures: cubic-core and monoclinic-shell. The time evolutions of the particle size and shell thickness indicated that the core was rapidly (but not instantaneously) formed at the initial stage of the precipitation process, followed by a slower shell growth. In addition, the solubility of the cubic core was estimated to be about 2.5 times higher than that of the monoclinic shell, resulting in the preferential dissolution of the interior of the particle by the washing process. The formation procedure has been used to construct multiple-shell hollow Mn-HCF particles containing up to quadruple separated nesting shells by associating an additional growth technique.
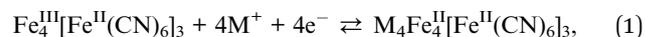
1. Introduction

Particulate materials with characteristic internal structures have attracted recent interest, and hollow particles are one of these kinds. For example, the large specific surface area of hollow particles is expected to improve electrochemical properties as electrode materials for secondary-batteries/capacitors,[1–7] electrochemical sensors,[8] or catalysts for oxygen evolution reaction.[9,10] The hollow space is applicable as a nanocontainer for loading functional molecules such as enzymes or anticancer agents for drug-delivery systems.[11–13]

For the preparation of hollow particles, Prussian blue (PB) and its analogs (PBAs) seem to be of greater importance.[14] PB is an artificial blue pigment composed of iron(III) and hexacyanoferrate(II) ions, typically $Fe_4[Fe(CN)_6]_3$ (omitting crystalline water molecules). Most PB and PBAs have a cubic crystal structure in which the metal and hexacyanoferrate ions are

alternatively aligned such as Na^+ and Cl^- ions in the rock salt structure. This is due to the structure of hexacyanoferrate ions, in which six CN^- ions coordinate with a Fe ion perpendicular to each other. Reflecting the cubic crystal structure, PBAs (including PB) tend to be in a cubic outer shape.[15–18] Although differences in the lattice constants are not so large, manganese hexacyanoferrate (Mn-HCF, the substance focused in this study) has exceptional crystal polymorphs such as monoclinic[19] or orthorhombic[20] structures in addition to the cubic one.[20,21]

Another crystallographic feature of PBAs is the large interstitial space resulting from CN bridges between metal and Fe ions such as metal–organic frameworks (MOFs). The large interstitial space, where the cations M^+, such as K^+, get into, rest, and come out, allow the PB redox reaction,

$$Fe_4^{III}[Fe^{II}(CN)_6]_3 + 4M^+ + 4e^- \rightleftarrows M_4Fe_4^{II}[Fe^{II}(CN)_6]_3, \quad (1)$$

without changing the crystal lattice, resulting in high durability for the repetition.[22]

Due to the redox property, PBAs have been studied for numerous electrochemical applications, including secondary-batteries,[3–7,22–24] electrochromic displays,[25–28] and electrochemical sensors.[8] Similar to other PBAs, Mn-HCF is also expected to be applied in Li^+ or Na^+-ion secondary batteries.[22,29–32] Particularly, the PBA structure seems to be advantageous for Na^+-ion batteries because the interaction of Na^+ ions with CN^- frameworks in PBAs are weaker than those with O^{2-} frameworks in oxides or phosphates, in addition to the presence of large interstitial space.[30] Besides, PBAs are also expected to be

[a]Department of Materials Science, Graduate School of Engineering, Chiba University, 1-33 Yayoicho, Inageku, Chiba 263-8522, Japan. E-mail: shiba@faculty.chiba-u.jp

[b]Department of Image and Materials Science, Graduate School of Advanced Integration Science, Chiba University, 1-33 Yayoicho, Inageku, Chiba 263-8522, Japan

[c]Department of Image Science, Faculty of Engineering, Chiba University, 1-33 Yayoicho, Inageku, Chiba 263-8522, Japan

applied for medical purposes such as cancer therapies.[33] For example, due to the magnetic property, PBAs are used as MRI contrast agents,[16,34] and due to the infrared absorption property, PB is applied for *in vivo* bioimaging[35] and photothermal therapy.[36,37]

For some hollow particles of metal oxides, *etc.*, PBA has been employed as the precursor material. Liu *et al.* obtained hollow $FeCo_2O_4$ particles by calcining cobalt hexacyanoferrate (Co-HCF) particles in the presence of a surfactant at 500 °C.[2] Ion-exchange $[Fe(CN)_3]^{4-}$ in PB (*i.e.*, Fe-HCF) with OH^- or MO_3^{2-} yields hollow $Fe(OH)_3$ or Fe_2O_3/MO_x particles, respectively, where M^{4+} denotes a tetravalent cation such as Sn^{4+} or Ge^{4+}.[1] The conversion of PBA particles into hollow metal phosphides[10] and selenides[9] has also been reported.

Hollow PB and PBA particles have been prepared *via* numerous procedures. Droplets in an emulsion are available to be used as a template for hollow PBA particles. Metal ions are introduced in an emulsion formed with ionomers that bind $[Fe(CN)_5]^{3-/4-}$ at the ends, causing the PBA shell formation.[14,38–41] Solid particles have been employed more commonly as cores, removed after the shells are formed. The solid cores are required to have different dissolution characteristics from the shells for their selective dissolution. One way is using substances other than PBA, such as Au[42] or SiO_2.[5] Even PBA is available as the core if the solubility is relatively higher than that for the shell, depending on the compositional differences, as in the $Mn_3[Fe(CN)_6]_2$ core for the $RbCo[Fe(CN)_6]$ shell.[43] Mn^{2+} ions in $Mn_3[Fe(CN)_6]_2$ can be ion-exchanged with Co^{2+} ions to form Co-HCF hollow particles also based on the solubility difference.[4]

Even single composition PBA particles are available for transforming them into hollow particles. Etching PB particles in HCl at 140 °C results in a hollow structure.[11,12,44] In this case, polyvinylpyrrolidone (PVP) adsorbed on the PB surface is considered to protect the shell from dissolution. Hollow Mn-HCF particles have been formed by the etching process in the sodium citrate solution that contains PVP.[13] Etching Ni-HCF with NH_3 yields hollow particles, even in the absence of PVP or other protecting agents.[8,9]

In the case of Mn-HCF, single-crystalline hollow particles have been obtained just by washing Mn-HCF particles with pure water.[3,6,45] Although PVP could be acting as a protecting agent[45] or a soft-template[6] for hollow structure formation, the presence of PVP might not be the essential factor since hollow Mn-HCF particles have been obtained even in the absence of PVP when the particles are precipitated *via* the reaction of Mn^{2+} and $[Fe(CN)_6]^{3-}$ in the presence of trisodium citrate (Na_3-Cit).[3] Compared to etching with HCl or NH_3, washing with pure water may be a preferred treatment to remove the core-part to form the hollow structure. Thus, the controversy on the Mn-HCF hollowing mechanism is worth resolving to evolve a mild procedure.

In this study, the authors reconsidered the precipitation process of Mn-HCF in the presence of Na_3-Cit to inspect the essential reason for the preferential dissolution of the core-part. Also, we propose an application of the procedure for the construction of hollow Mn-HCF particles with multiple-shells that have up to quadruple separated nesting shells, as in a matryoshka-doll, by associating with an additional growth technique.

2. Experimental

2.1 Materials

The reagents used ($MnCl_2 \cdot 4H_2O$, $K_3[Fe(CN)_6]$, and trisodium citrate dihydrate) were of analytical grade and purchased from Wako Pure Chemicals, Osaka, Japan. A deionized bovine bone gelatin was provided by Nitta Gelatin, Osaka, Japan. These chemicals were used as-received without further purification.

2.2 Preparation of single-shell hollow Mn-HCF particles

The precipitation process was carried out at 25 °C in a water bath. Under magnetic stirring conditions, 2.5 mL of 0.075 mol L^{-1} $MnCl_2$ and then 2.5 mL of 0.050 mol L^{-1} of $K_3[Fe(CN)_6]$ aqueous solutions were introduced into 20 mL of a 0.025 mol L^{-1} Na_3-Cit aqueous solution and typically reacted for 40 min. The precipitate was separated using a centrifuge (10 000 rpm, 15 min). The precipitate was re-dispersed in distilled water and centrifuged again, this washing process was repeated 4 times to obtain hollow particles.

Instead of using the centrifuge, suction filtration was employed for the solid–liquid separation process when inspecting the formation process. After suction filtration with a membrane filter (cellulose acetate, pore size 0.2 μm), the precipitate was rinsed three times with a small amount of cold distilled water to obtain as-prepared particles. To convert the as-prepared particles into hollow ones, they were re-dispersed in 50 mL distilled water ultrasonically and then filtered again; this process was repeated once more.

2.3 Construction of multiple-shell hollow particles

An additional growth (or seeded growth) technique[46] was used to produce another shell on the outer side of each seed hollow particle. Single-shell hollow seed particles were prepared basically by the procedure described in Section 2.2, with 1.6 times the volume (reaction time 40 min). At 20 min, 1.6 mL of a 1% gelatin solution was added to the reacting sol to prevent agglomeration among the particles during the following solid–liquid separation process *via* suction filtration. The separated particles were then washed in distilled water *via* ultrasonic irradiation, as described above, to obtain the hollow particles. The hollow particles were re-dispersed in 5 mL of distilled water to be the seed dispersion.

The double-shell hollow particles were obtained as follows. 4 mL of seed dispersion was added to 18.5 mL of an aqueous solution that contained 0.027 mol L^{-1} Na_3-Cit and 0.010 mol L^{-1} $MnCl_2$. Then, at 25 °C, under magnetic stirring, 2.5 mL of 0.050 mol L^{-1} $K_3[Fe(CN)_6]$ aqueous solution was introduced to form the additional Mn-HCF layer around the hollow particles. At 20 min, 1 mL of 1% gelatin solution was added, and the particles were collected at 40 min by suction filtration. The particles were converted to a double-shell structure by washing with distilled water in the same manner. Repeating the additional growth process, triple- and quadruple-shell hollow particles were also prepared using the double- and triple-shell ones, respectively, as the seed.

Paper

2.4 Analysis

The particle size and morphology were evaluated using a transmission electron microscope (TEM; Hitachi H-7650, operated at 100 kV) and a field-emission scanning electron microscope (FE-SEM; JEOL JSM-6700F, operated at 15 kV). To prepare TEM specimens, a small amount of the as-prepared precipitate was dispersed in 2-propanol, whereas distilled water was used for hollow particles. The size of each particle was measured from the printed TEM images with a vernier caliper. For the FE-SEM observation, the precipitate was directly put on a piece of aluminum foil just after centrifugation and then dried; the specimen was coated with Pt.

The crystal structure was analyzed *via* powder X-ray diffraction with the freeze-dried samples (XRD; Bruker D8 Advance, Cu Kα radiation λ = 1.5418 Å); the selected area electron diffraction (SAED) patterns were also taken with TEM. Energy-dispersive X-ray spectroscopy was employed to estimate the elemental composition of the particles (EDX; EDAX Genesis XM2T attached to the TEM). Concentrations of Mn and Fe in the aqueous phase were measured *via* atomic absorption spectroscopy (AA; Varian SpectrA55; C_2H_2/air flame).

3. Results and discussion

3.1 Single-shell hollow particles prepared without PVP

Fig. 1 shows TEM and FE-SEM images of the single-shell hollow Mn–HCF particles prepared by the present procedure (reaction time 40 min). The TEM image of each particle in Fig. 1a is a square frame silhouette with the lower-contrast inner plane. As the intensity of scattering contrast on the TEM image reflects the path length through which the electron beam is passing, the silhouettes in Fig. 1a result from the difference in the thickness of the substance towards the vertical direction to the image. On the other hand, the outer shape of the particles is cubic, as seen from the SEM image in Fig. 1b; as such, the TEM image in Fig. 1a implies a hollow structure for the particles. This hollow structure is indicated more directly by an FE-SEM image of a cracked particle shown in Fig. 1c.

The particle size was estimated to be 474 nm ± 86 nm in the mean size ± one standard deviation estimated from about 250 individual particles on TEM images. The thickness of the shell was 50 nm ± 16 nm. The elemental composition evaluated by TEM-EDX measurements was $K_{1.37}Mn_{1.11}[Fe(CN)_6]$ (see ESI†).

The mean valence of Fe, +2.41, was calculated from the composition by considering the charge balance between cations (K^+ and Mn^{2+}) and anions ($[Fe^{II}(CN)_6]^{4-}$ and $[Fe^{III}(CN)_6]^{3-}$). The mean valence suggests that at least half $[Fe^{III}(CN)_6]^{3-}$ ions in the particles were reduced to $[Fe^{II}(CN)_6]^{4-}$ during the precipitation process.

Fig. 2 indicates the structural analyses of the hollow particles. The peaks in the XRD pattern, as shown in Fig. 2a, appear to be matched with either the monoclinic structure (PDF 01-089-8979; $P2_1/c$; $a = 10.108$ Å, $b = 10.104$ Å, $c = 10.114$ Å, $\beta = 92.93°$) or the cubic one (PDF 00-046-0910; $F\bar{4}3m$; $a = 10.061$ Å) of Mn-HCF. However, the SAED pattern in Fig. 2b supports the monoclinic structure since the pattern indicates 012 reflections, which are allowed for the monoclinic structure but forbidden for the cubic one. The monoclinic structure has also been concluded in the literature.[45] Although the characteristic peaks of $\bar{2}02$ and 202 reflections for the monoclinic structure, expected at 24.3° and 25.6°, respectively, are not evident in Fig. 2a, the peaks appeared when the reaction time was extended, as discussed later. The Laue spots in Fig. 2b imply a well-oriented, single-crystalline arrangement of the atoms. The HR-TEM image in Fig. 2c, which shows orthogonal lattice images with 5.1 Å separation, also confirms this. Note that the present hollow Mn-HCF particles do not require PVP during both the precipitation and washing processes.

3.2 Formation process evaluation for the hollow structure

TEM images in Fig. 3 indicate the time evolution of the particles until 360 min. The silhouettes of the as-prepared particles seem to have no specific internal textures at each reaction time. Even at 10 min, the particle size was as large as 462 nm on average,
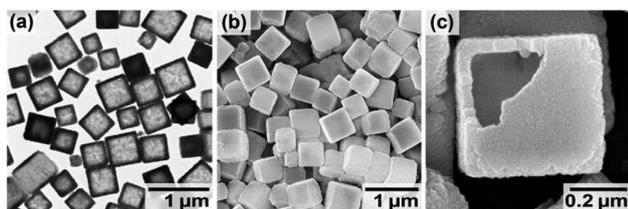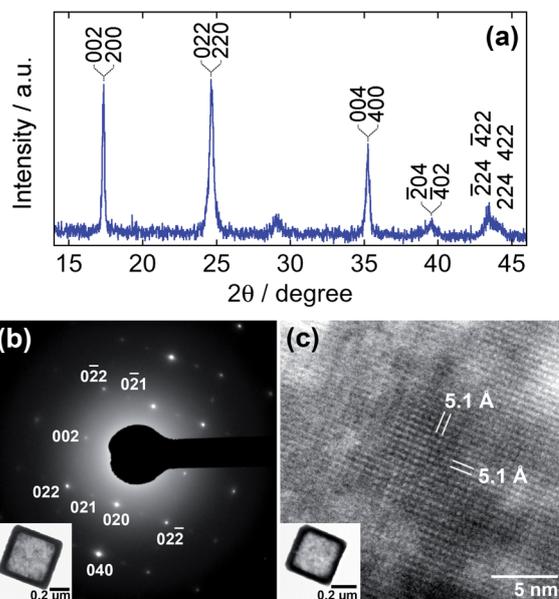

Fig. 1 Electron micrographs of the hollow Mn–HCF particles prepared with MnCl₂ and K₃[Fe(CN)₆] aqueous solutions in the presence of Na₃-Cit, followed by washing with distilled water. (a) TEM image, (b) SEM image, and (c) SEM image of a cracked particle showing the internal hollow space.

Fig. 2 Crystal structure analyses of the hollow Mn–HCF particles. (a) XRD pattern (Cu Kα, λ = 1.5148 Å), (b) SAED pattern from the single particle in the inset, and (c) HR-TEM image at the center of the particle in the inset.
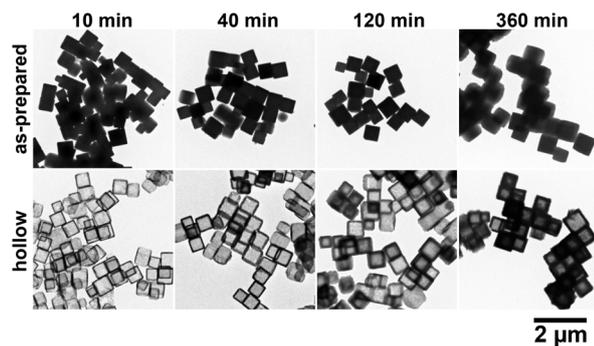
Fig. 3 TEM images of Mn-HCF particles at different reaction times. The as-prepared particles are shown in the upper row, and the lower row indicates the hollow particles obtained after washing the respective as-prepared particles with distilled water.

followed by a slower size increase to 592 nm at 360 min (corresponding to a 2.1 times increase in volume). The initial rapid growth agreed with the prompt (but not instantaneous) turbidity increase in the reacting sol after mixing of the reactant solutions. After washing the as-prepared particles with distilled water, the hollow structures were formed, as shown in the lower row in Fig. 3. The precipitate color was initially purple and turned white after washing. This apparently means that the washing treatment converted the as-prepared particles into hollow particles by dissolving the cores. It also seems from Fig. 3 that the shell was somewhat imperfect at 10 min and the thickness increased with reaction time.
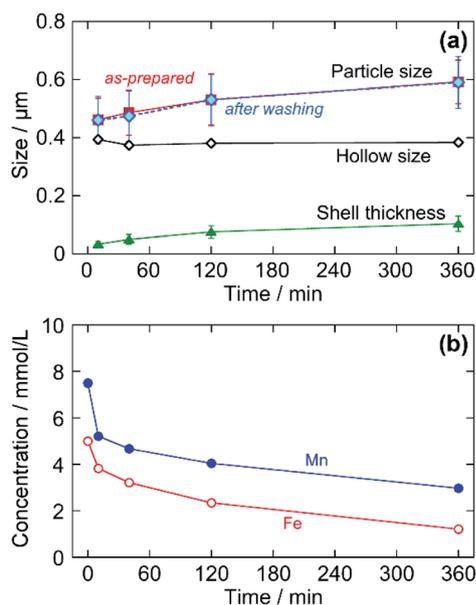

Fig. 4 Time evolutions of the particle size and the reactant concentration during the formation process of the Mn-HCF particles. (a) Mean particle size (edge length) of the as-prepared ones (■), that of the hollow particles after washing (◆), and mean shell thickness (▲), where the error bars indicate one standard deviation. The hollow size (◇) is calculated from the mean values of particle size and the shell thickness. (b) Concentrations of Mn (●) and Fe (○) remaining in the aqueous phase.

The growth behavior is indicated in Fig. 4 in detail. Fig. 4a shows time evolutions of the mean size (*i.e.*, edge length) and the mean shell thickness of particles estimated from the TEM observations. The particle size at each reaction time was unchanged through the washing process. Though both the mean particle size (L) and mean shell thickness (T) increased with time, the calculated size of the hollow, or the removed core, ($=L - 2T$) was almost constant during the formation process.

The reactants remaining in the aqueous phase were measured by AA (see ESI†). By the particle growth, the total concentrations of Mn and Fe remaining in the aqueous phase were decreased with reaction time (Fig. 4b); the conversions calculated by the decrease of Fe were 24%, 36%, 53%, and 76% at 10, 40, 120, and 360 min, respectively. These results imply that the as-prepared particles have a kind of core–shell structure with different solubilities. The core is promptly precipitated just after mixing the reactants, followed by the slow growth of the shell. The core is then dissolved to form the hollow space by the washing process.

The core–shell structure formation was confirmed by XRD by fine scanning just around the 220 reflection. Fig. 5 shows the XRD patterns for the as-prepared and hollow particles at some reaction times. Note that lacking the hollow particle's pattern at 10 min is due to the tiny sample amount. The peak at $2\theta = 24.5°$ for the as-prepared particles at 10 min is located at a slightly lower 2θ position than the 022 reflection of monoclinic Mn-HCF ($2\theta = 24.7°$). As the reaction time progressed, the intensity at $2\theta = 24.7°$ increased to be an additional peak. Besides, at 360 min, weak $\bar{2}02$ and 202 reflections from the monoclinic structure were observed at 24.2° and 25.3°, respectively. In addition, the peak at 24.7° remained, whereas that at 24.5° disappeared, after the washing process, converting the as-prepared particles into hollow ones. This behavior means that monoclinic Mn-HCF is stacked on the core of the Mn-HCF particle as the shell with a slightly smaller lattice parameter.

To identify the core crystal structure, XRD and SAED measurements were performed on Mn-HCF particles obtained
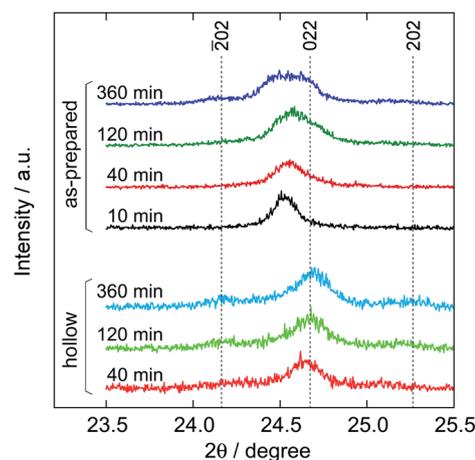

Fig. 5 Comparison of the XRD patterns among the as-prepared and hollow particles at various reaction times (Cu Kα radiation, $\lambda = 1.5418$ Å). The indexes of reflection are of monoclinic Mn-HCF. Intensities for the hollow particles are indicated by being doubled.

by separating from the aqueous phase at 2 min of the reaction time by suction filtration; the particles were expected to have almost no shell-part yet at this reaction time, as shown in Fig. 4a. After rinsing three times with small amounts of cold distilled water, a bit of the precipitate was dispersed in 2-propanol to be a TEM specimen for SAED; the remainder was freeze-dried for XRD.

Fig. 6 shows the XRD and SAED patterns from the *core particles*, as indicated in the respective insets. The XRD peaks in Fig. 6a can be indexed to a cubic structure with $a = 10.275$ Å. Note that $\bar{2}02$ and 202 reflections from monoclinic Mn-HCF are not found in the pattern. The Laue spots from SAED in Fig. 6b support the cubic structure since there seem to be no reflections such as 021, 110, and 130 ones, which are forbidden for the cubic Mn-HCF but are allowed for the monoclinic structure. Therefore, it is reasonable to conclude that the as-prepared Mn-HCF particles possess a cubic structure in the core; the lattice parameter, $a = 10.275$ Å, seems to be somewhat larger than that for cubic Mn-HCF as reported in the literature ($Mn_2[Fe(CN)_6]\cdot 0.5H_2O$; $a = 10.061$ Å; PDF 00-046-0910), probably due to the difference in the cation composition.

The estimated solubility were 1.5×10^{-4} mol L^{-1} for the core of cubic Mn-HCF and 6×10^{-5} mol L^{-1} for the shell of monoclinic Mn-HCF, supporting the preferential dissolution of the core due to the solubility difference between the crystal structures. Note that excessive washing will dissolve the shells to make them collapse as the solubility difference is only about 2.5 times. Note also that the measured solubility might be somewhat larger than the bulk solids due to the Gibbs–Thomson effect, which indicates that smaller particles have higher solubility.[47] Even so, the hollow particle formation is still attributed to the core's higher solubility since the mean size of the *core particles* shown in Fig. 6a is similar to that indicated in Fig. 4a, and since the *shell particles* are the hollow ones.
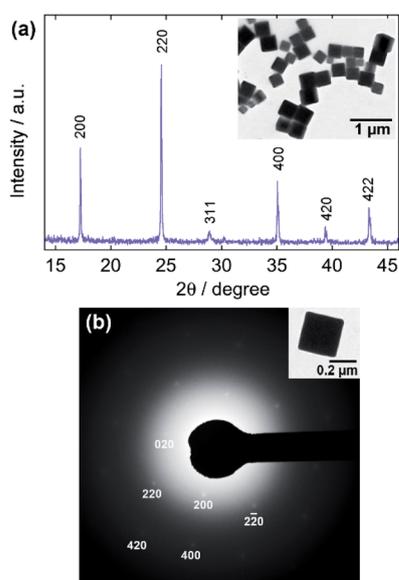

Fig. 6 Diffractometric analysis of the Mn–HCF particles to be the core of the as-prepared ones. (a) XRD pattern using Cu Kα radiation, $\lambda = 1.5418$ Å. (b) SAED pattern from the single particle in the inset.

These solubility values might seem to be much smaller than the Mn concentration shown in Fig. 4b. However, they are rather reasonable if we take into account the complex formation with citrate ions. The free Mn^{2+} concentration, $[Mn^{2+}]$, is estimated to be 8.5×10^{-5} mol L^{-1} at 10 min under the reacting pH of 6.44, where stability constants for MnL^- and $MnHL$ complexes are $\beta_{ML} = 4.7 \times 10^3$ L mol^{-1} and $\beta_{MHL} = 1.2 \times 10^2$ L mol^{-1}, respectively,[48,49] and the dissociation constant for citric acid pK_{as3} 5.68,[50] where L^{3-} denotes citrate ion (see ESI†).

Although the formation mechanism for the core–shell particles with a different crystal structure is not clear yet, the great difference in the formation rates could relate to this. As shown in Fig. 4, the constant hollow size during the precipitation process suggests that the core formation is a rapid process completing within 10 min. In contrast, the shell formation is a much slower process as the thickness is still increasing even at 360 min. The slower deposition rate of the monoclinic phase could allow the cubic phase precipitation before the shell formation from the highly supersaturated solution in spite of the lower solubility of the monoclinic phase. Even when the reactant concentrations reach the solubility level for cubic Mn-HCF, the solution should still be supersaturated for the monoclinic Mn-HCF. Therefore, the monoclinic phase would slowly deposit as the shell on the cubic Mn-HCF particles of the core.

For the core formation step, $[Fe^{III}(CN)_6]^{3-}$ seems to be reduced to $[Fe^{II}(CN)_6]^{4-}$, as the Fe's valence was estimated as, for example, +2.18 for the as-prepared particle at 10 min from the TEM-EDX result, $K_{1.47}Mn_{1.20}[Fe(CN)_6]$ (Fig. S2 in ESI†). However, the free $[Fe^{III}(CN)_6]^{3-}$ ion was not reduced by the citrate ion under the present conditions (Fig. S3 in ESI†) such that it was unlikely to occur in a stepwise process in which $[Fe^{III}(CN)_6]^{3-}$ was first reduced to $[Fe^{II}(CN)_6]^{4-}$ and then reacted with Mn^{2+}. Rather, an Mn^{2+}-citrate complex seems to be acting as the precursor since about 98% of Mn^{2+} in the aqueous phase was expected as in the citrate-complex form. An electron could be transferred from an Mn^{2+}-citrate complex to a $[Fe(CN)_6]^{3-}$ ion to form an Mn^{2+}-$[Fe(CN)_6]^{4-}$ unit to precipitate Mn-HCF promptly. This process would proceed until the system reaches the solubility level for the cubic Mn-HCF.

On the shell formation step, the chemical reaction would basically be the same as for the core formation since the conditions other than the supersaturation level were maintained. The monoclinic Mn-HCF was deposited slowly under a lower supersaturation ratio. Besides, in the supernatant solution from which Mn-HCF particles were removed at 40 min, large monoclinic Mn-HCF particles were generated at a similar formation rate to the shell formation (Fig. S4 in ESI†). The Fe's valence of the shell at 40 min (+2.41) was somewhat higher than that of the core (+2.18), suggesting the co-precipitation of $[Fe(CN)_6]^{3-}$ and $[Fe(CN)_6]^{4-}$ with Mn^{2+} on the shell formation step. However, the Fe's valence of the shell decreased with reaction time (+2.38 at 120 min and +2.25 at 360 min). The co-precipitated $[Fe(CN)_6]^{3-}$ could be reduced even after deposition.

3.3 Construction of multiple-shell hollow particles

At the end of this study, we have constructed multiple-shell hollow particles that contain up to quadruple separated
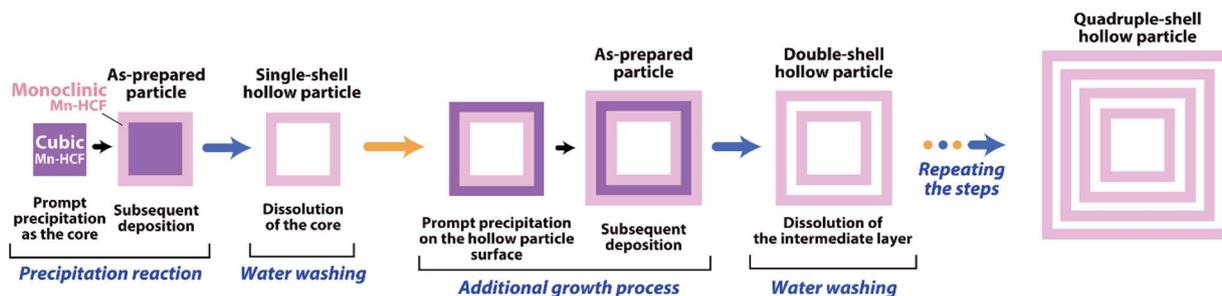
Fig. 7 Schematic explaining the construction process of multiple-shell hollow Mn-HCF particles. In the additional growth process, also, the cubic Mn-HCF promptly precipitates on the hollow particle surface, followed by the subsequent deposition of monoclinic Mn-HCF. Removing the sandwiched cubic Mn-HCF layer results in the multiple-shell hollow structure with the monoclinic Mn-HCF shells.
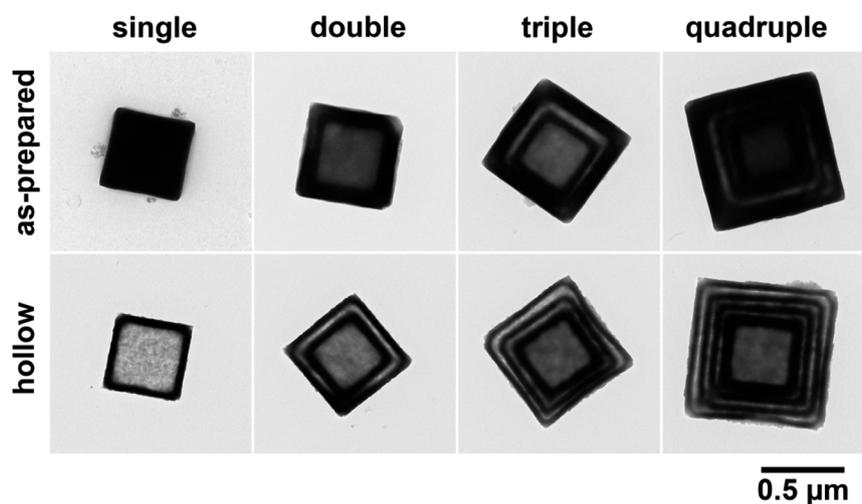

Fig. 8 TEM images of the formation of multiple-shell hollow Mn-HCF particles by applying the additional growth procedure. The as-prepared particles are shown in the upper row, and the respective hollow particles after washing are in the lower row.

nesting Mn-HCF shells. As illustrated in Fig. 7, the present preparation procedure is combined with an additional growth technique.[46] The precipitation reaction was carried out in the presence of single-shell hollow particles, and the cubic Mn-HCF phase is promptly formed on hollow particle surfaces, followed by the subsequent monoclinic Mn-HCF phase deposition on the cubic Mn-HCF. The sandwiched cubic Mn-HCF phase of each particle is dissolved to form a double-shell hollow particle by washing with distilled water. Repeating these processes produce the triple- and quadruple-shell hollow particles.

Fig. 8 shows the TEM images of the multiple-shell particles constructed by this procedure, where those in the upper and lower rows are before and after washing with distilled water, respectively (also see Fig. S5 and S6 in ESI†). Each additional growth process increased the shell thickness by depositing the Mn-HCF layer on the surface of the seed hollow particles. Accordingly, hollow spaces (about 40 nm) were formed in the middle part of the grown shells by washing with distilled water. As a result, nesting-doll structure particles were formed with concentric shells of 40–50 nm thick. These results suggest that even in the additional growth process, cubic Mn-HCF is first deposited on the seed's surface, followed by the deposition of

monoclinic Mn-HCF on the cubic Mn-HCF, similar to the single-shell hollow particle formation.

Dispersing the seed particles is generally important for additional growth processes to maintain the size distribution width. If two (or more) seed hollow particles contact each other during the additional growth step, the deposited layer surrounds the pair of particles, resulting in two-in-one hollow particles, as shown in Fig. S7 in ESI.† Although such particles might have another importance, the occurrence frequency should be reduced to avoid spreading the size and structural distributions of the multiple-shell hollow particles. Introducing a small amount of gelatin before the solid–liquid separation improved the seed dispersion and the quality of the multiple-shell hollow particles in the present system.

4. Conclusions

In this study, the formation process has been considered for the hollow Mn-HCF particles precipitated from an aqueous solution containing $MnCl_2$ and $K_3[Fe(CN)_6]$ in the presence of sodium citrate. The as-prepared particles transform into the hollow ones by washing with distilled water. The XRD and SAED

measurements suggested that the as-prepared particle has a core–shell structure with the cubic and monoclinic crystal structures for the core and shell, respectively. The core's solubility was estimated as about 2.5 times higher than that of the shell, resulting in its preferential dissolution. Up to quadruple-shell hollow Mn-HCF particles have also been constructed based on this procedure associated with the additional growth technique.

Conflicts of interest

There are no conflicts to declare.

Acknowledgements

References

1 L. Zhang, H. B. Wu and X. W. Lou, *J. Am. Chem. Soc.*, 2013, **135**, 10664–10672.

2 L. Liu, Z. Hu, L. Sun, G. Gao and X. Liu, *RSC Adv.*, 2015, **5**, 36575–36581.

3 X. Jiang, H. Liu, J. Song, C. Yin and H. Xu, *J. Mater. Chem. A*, 2016, **4**, 16205–16212.

4 J.-G. Wang, Z. Zhang, X. Zhang, X. Yin, X. Li, X. Liu, F. Kang and B. Wei, *Nano Energy*, 2017, **39**, 467–653.

5 A. Azhar, M. B. Zakaria, E. M. Ebeid, T. Chikyow, Y. Bando, A. Alshehri, Y. G. Alghamdi, Z.-X. Cai, N. A. Kumar, J. Lin, H. Kim and Y. Yamauchi, *ChemistryOpen*, 2018, **7**, 599–603.

6 Y. Huang, M. Xie, Z. Wang, Y. Jiang, Y. Yao, S. Li, Z. Li, L. Li, F. Wu and R. Chen, *Small*, 2018, **14**, 1801246.

7 Y. Ye, L. Yu, M. Sun, G. Cheng, S. Fu, S. Peng, S. Han and X. Yang, *Electrochim. Acta*, 2019, **319**, 237–244.

8 Q. Niu, C. Bao, C. Cao, C. Liu, H. Wang and W. Lu, *Biosens. Bioelectron.*, 2019, **141**, 111445.

9 J. Nai, Y. Lu, L. Yu, X. Wang and X. W. Lou, *Adv. Mater.*, 2017, **29**, 1703870.

10 X. Ding, W. Uddin, H. Sheng, P. Li, Y. Du and M. Zhu, *J. Alloys Compd.*, 2020, **814**, 152332.

11 L. Jing, S. Shao, T. Wang, Y. Yang, X. Yue and Z. Dai, *Theranostics*, 2016, **6**, 40–53.

12 J. Zhou, M. Li, Y. Hou, Z. Luo, Q. Chen, H. Cao, R. Huo, C. Xue, L. Sutrisno, L. Hao, Y. Cao, H. Ran, L. Lu, K. Li and K. Cai, *ACS Nano*, 2018, **12**, 2858–2872.

13 Q. Jia, F. Su, Z. Li, X. Huang, L. He, M. Wang, Z. Zhang, S. Fang and N. Zhou, *ACS Appl. Bio Mater.*, 2019, **2**, 2143–2154.

14 L. Catala and T. Mallah, *Coord. Chem. Rev.*, 2017, **346**, 32–61.

15 X. Wu, M. Cao, C. Hu and X. He, *Cryst. Growth Des.*, 2006, **6**, 26–28.

16 M. Shokouhimehr, E. S. Soehnlen, J. Hao, M. Griswold, C. Flask, X. Fan, J. P. Basilion, S. Basu and S. D. Huang, *J. Mater. Chem.*, 2010, **20**, 5251–5259.

17 F. Shiba, R. Fujishiro, T. Kojima and Y. Okawa, *J. Phys. Chem. C*, 2012, **116**, 3394–3399.

18 F. Shiba, U. Mameuda, S. Tatejima and Y. Okawa, *RSC Adv.*, 2019, **9**, 34589–34594.

19 G. Małecki and A. Ratuszna, *Powder Diffr.*, 1999, **14**, 25–30.

20 R. Martínez-García, E. Reguera, J. Rodriguez, J. Balmaseda and J. Roque, *Powder Diffr.*, 2004, **19**, 255–264.

21 S. Juszczyk, C. Johansson, M. Hanson, A. Ratuszna and G. Małecki, *J. Magn. Magn. Mater.*, 1994, **138**, 281–286.

22 M. J. P. Muñoz and E. C. Martínez, *Prussian Blue Based Batteries*, Springer, Cham, Switzerland, 2018.

23 H. Minowa, Y. Yui, Y. Ono, M. Hayashi, K. Hayashi, R. Kobayashi and K. I. Takahashi, *Solid State Ionics*, 2014, **262**, 216–219.

24 Y. Lu, L. Wang, J. Cheng and J. B. Goodenough, *Chem. Commun.*, 2012, **48**, 6544–6546.

25 V. D. Neff, *J. Electrochem. Soc.*, 1978, **125**, 886–887.

26 S. Hara, H. Tanaka, T. Kawamoto, M. Tokumoto, M. Yamada, A. Gotoh, H. Uchida, M. Kurihara and M. Sakamoto, *Jpn. J. Appl. Phys.*, 2007, **46**, L945–L947.

27 A. Paolella, C. Faure, V. Timoshevskii, S. Marras, G. Bertoni, A. Guerfi, A. Vijh, M. Armand and K. Zaghib, *J. Mater. Chem. A*, 2017, **5**, 18919–18932.

28 S. Kimura, K. Nakamura and N. Kobayashi, *Sol. Energy Mater. Sol. Cells*, 2020, **205**, 110247.

29 N. Imanishi, T. Morikawa, J. Kondo, R. Yamane, Y. Takeda, O. Yamamoto, H. Sakabe and M. Tabuchi, *J. Power Sources*, 1999, **81–82**, 530–534.

30 L. Wang, Y. Lu, J. Liu, M. Xu, J. Cheng, D. Zhang and J. B. Goodenough, *Angew. Chem., Int. Ed.*, 2013, **52**, 1964–1967.

31 Y. Kurihara, T. Matsuda and Y. Morimoto, *Jpn. J. Appl. Phys.*, 2013, **52**, 017301.

32 M. Pasta, C. D. Wessells, N. Liu, J. Nelson, M. T. McDowell, R. A. Huggins, M. F. Toney and Y. Cui, *Nat. Commun.*, 2014, **5**, 3007.

33 M. Gautam, K. Poudel, C. S. Yong and J. O. Kim, *Int. J. Pharm.*, 2018, **549**, 31–49.

34 M. Shokouhimehr, E. S. Soehnlen, A. Khitrin, S. Basu and S. D. Huang, *Inorg. Chem. Commun.*, 2010, **13**, 58–61.

35 R. Weissleder, *Nat. Biotechnol.*, 2001, **19**, 316–317.

36 G. Fu, W. Liu, S. Feng and X. Yue, *Chem. Commun.*, 2012, **48**, 11567–11569.

37 P. Xue, L. Sun, Q. Li, L. Zhang, Z. Xu, C. M. Li and Y. Kang, *J. Colloid Interface Sci.*, 2018, **509**, 384–394.

38 G. Liang, J. Xu and X. Wang, *J. Am. Chem. Soc.*, 2009, **131**, 5378–5379.

39 R. McHale, N. Ghasdian, Y. Liu, M. B. Ward, N. S. Hondow, H. Wang, Y. Miao, R. Brydson and X. Wang, *Chem. Commun.*, 2010, **46**, 4574–4576.

40 X. Roy, J. K.-H. Hui, M. Rabnawaz, G. Liu and M. J. MacLachlan, *J. Am. Chem. Soc.*, 2011, **133**, 8420–8423.

41 R. McHale, Y. Liu, N. Ghasdian, N. S. Hondow, S. Ye, Y. Lu, R. Brydson and X. Wang, *Nanoscale*, 2011, **3**, 3685–3694.

42 G. Maurin-Pasturel, J. Long, Y. Guari, F. Godiard, M.-G. Willinger, C. Guerin and J. Larionova, *Angew. Chem., Int. Ed.*, 2014, **53**, 3872–3876.

43 O. N. Risset, E. S. Knowles, S. Ma, M. W. Meisel and D. R. Talham, *Chem. Mater.*, 2013, **25**, 42–47.

44 M. Hu, S. Furukawa, R. Ohtani, H. Sukegawa, Y. Nemoto, J. Reboul, S. Kitagawa and Y. Yamauchi, *Angew. Chem.*, 2012, **124**, 1008–1012.

45 M. Hu, N. L. Torad and Y. Yamauchi, *Eur. J. Inorg. Chem.*, 2012, 4795–4799.

46 F. Shiba, M. Nito, K. Kawakita and Y. Okawa, *Part. Sci. Technol.*, 2015, **33**, 671–676.

47 T. Sugimoto and F. Shiba, *J. Phys. Chem. B*, 1999, **103**, 3607–3615.

48 A. E. Martell, in *Stability Constants of Metal-Ion Complexes*, ed. L. G. Sillén and A. E. Martell, Special Publication No. 17, The Chemical Society, London, 1964, p. 479.

49 N. C. Li, A. Lindenbaum and J. M. White, *J. Inorg. Nucl. Chem.*, 1959, **12**, 122–128.

50 E. Campi, G. Ostacoli, M. Meirone and G. Saini, *J. Inorg. Nucl. Chem.*, 1964, **26**, 553–564.